# ON THE SOLUTION OF GEOMETRIC PDES ON SINGULAR DOMAINS VIA THE CLOSEST POINT METHOD

by

Parousia Rockstroh

B.Sc., Harvey Mudd College, 2008

a Thesis submitted in partial fulfillment
of the requirements for the degree of
Master of Science
in the Department of Mathematics
Faculty of Science


SIMON FRASER UNIVERSITY
Fall 2011

## APPROVAL

| | |
|---|---|
| **Name:** | Parousia Rockstroh |
| **Degree:** | Master of Science |
| **Title of Thesis:** | On the Solution of Geometric PDEs on Singular Domains via the Closest Point Method |
| **Examining Committee:** | Dr. John Stockie, Associate Professor<br>(Chair) |
| | Dr. Steven Ruuth, Professor<br>Senior Supervisor |
| | Dr. Nilima Nigam, Associate Professor<br>SFU Examiner |
| | Dr. Adam Oberman, Associate Professor<br>External Examiner |
| **Date Approved:** | December 7th, 2011 |

# Declaration of
# Partial Copyright Licence

# Abstract

In this thesis we present several new techniques for evolving time-dependent geometric-based PDEs on surfaces. In particular, we construct a method for posing and subsequently solving a PDE on a given manifold $M$ by using the Riemann metric tensor and the definition of the Laplace-Beltrami operator in local coordinates to lift the differential structures to another manifold $\tilde{M}$, which is constructed via a prescribed method. This allows for an innovative method of solving PDEs on manifolds. In addition, we explore an algebraic-geometric approach to resolving singularities that may arise on manifolds. Ultimately, these techniques are developed with a view to solving time-dependent PDEs that are defined on domains containing singularities by means of the closest point method.

*To my family.*

*"Vox clamantis in deserto"*

— *Vulgate*, Iohanni, *90 AD*

# Acknowledgments

I would like to thank my advisor, Professor Steven J. Ruuth, for providing help, guidance, advice, and insight throughout the course of this project. As one of the creators of the closest point method, he has provided a great deal of insight into the inner-workings of the method. I would also like to thank Professors Nilima Nigam and Adam Oberman for reading initial drafts of this thesis and providing many helpful comments and suggestions. I would like to thank Professor Ailana Fraser at the University of British Columbia for providing insight into some of the geometric aspects of the theory presented in this thesis. Her help and guidance has contributed to the rigour of many of the geometrical details that are presented. I would also like to thank Professor Colin MacDonald from the University of Oxford for proposing an initiating a discussion that led to my pursuit of much of this research.

# Contents

# List of Figures

# Preface

The goal of this thesis is twofold in nature: first, we seek to give an expository account of the geometric ideas and principles behind the closest point method, and second we wish to present original research on the numerical solution of time-dependent PDEs on domains with singularities. The former is in large part for the sake of future generations who may study and use the closest point method, while the latter is for the explicit purpose of extending the method to incorporate a wider class of problems that are now solvable as a consequence of the results in this thesis.

It has become increasingly common in modern scientific disciplines to pose problems involving partial differential equations (PDEs) on surfaces that are often non-cartesian. Such applications include the diffusion of heat or substances across interfaces, the segmentation of images on surfaces, the deformation of solid objects, and the computation of eigenvalues on manifolds embedded in $\mathbb{R}^3$. All of these problems require the solution of PDEs that are posed on complex geometries.

When approaching problems in continuous mathematics, it is natural to attempt a direct analysis of the problem within the given mathematical framework. In the case of geometric PDEs defined on general compact Riemannian manifolds, in order to take such an approach, one must be equipped with the tools of modern differential geometry. Indeed, such work has been considered at least as early as the 1950s by S. Minakshisundaram and A. Pleijel in works such as [15], [16], and [17]. In this set of papers, the authors pose and subsequently explore the Laplace-Beltrami operator on compact Riemannian manifolds, and in the process derive several useful asymptotic estimates for the distribution of the eigenvalues of the operator. Ultimately, in [16], Minakshisundaram demonstrates a method for posing a heat

kernel on a Riemannian manifold by means of the eigenfunction expansions given in [17]. Other ideas of interest are also presented in [17] including the construction of a Riemann zeta function on a manifold, which in subsequent decades has been eponymously named the Minakshisundaram-Pleijel zeta function. It should be noted that although many of these notions are defined and constructed, the results that are presented in these papers do not readily lend themselves to practical calculations. In the decades that followed, many advances were made in the theory of geometric PDEs including results on the spectrum of the Laplace-Beltrami operator on general compact manifolds, a number of asymptotic estimates for special classes of manifolds, and further techniques for constructing kernels of geometric PDE operators on manifolds. An excellent summary of many of these developments is given by Isaac Chavel in [1] and [2].

Due to the complexity of many manifolds, it is difficult to develop solution techniques for PDEs on general manifolds. As a result a number of techniques have been developed in recent years to address the solution of PDEs on surfaces. One such method, which we will focus on in this thesis, is the closest point method. The closest point method was originally developed by Ruuth and Merriman in [14] and [18] and has been further developed by Ruuth and MacDonald in [13] and [12]. The closest point method has been applied to a number of problems including the diffusion of heat on surfaces, the segmentation of images on surfaces, and the computation of eigenvalues on surfaces in the aforementioned papers as well as in [11] and [19].

In previous works, however, the closest point method has not consider problems posed on domains with corners or singularities. Several questions both theoretical and computational have surrounded such problems since the creation of the closest point method. The contribution of the current work is to develop an extension of the closest point method that allows for computation of PDEs on domains containing singularities and corners. In the process several new techniques and methods for solving geometric PDEs are explored. Indeed, the solution of this problem itself relies on the interplay between the closest point method and the deep connections between the geometry of manifolds and the differential structures that are posed on them.

In chapter three we present a method from algebraic geometry for resolving singularities. The method known as 'blowing-up' a singularity resolves singularities by replacing the singular set of a given space by all possible directions pointing out of the subspace. This process is well-studied in algebraic geometry and can further be explored in references such as [5], [6], and [7]. In addition to presenting the blow-up technique, we propose a method for modifying differential operators defined on a given surface so that the resulting PDE corresponds to a flow on a related surface. This result is original to this thesis although much of the background need for the construction can be found in standard references such as [8] and [9] as well as [4]. Finally, in chapter four, we combine the aforementioned geometric techniques with the closest point method to construct a numerical method for evolving time-dependent PDEs on surfaces with singularities. The resulting numerical method is the primary result of the thesis and is original to this work.

# Chapter 1

# Analytic Approach to Solving PDEs on Manifolds

In this chapter we outline some of the foundational material from differential geometry and manifold theory that is needed to pose and solve PDEs on complex geometries. In the process we will consider the definition and examples of manifolds along with the differential structures that can be defined on them. This discussion will naturally lead to the construction of a fundamental solution of the heat equation on compact manifolds. The material in this chapter is meant to be self-contained. It is only assumed that the reader has a basic understanding of real analysis and point-set topology. In particular, it will be assumed that the reader is familiar with the separation axioms of topology and the definition of a homeomorphism. For an excellent reference on point-set topology the reader may want to see [**?**], and a standard reference for basic real analysis is [**?**]. We will now begin our discussion by giving the definition of a topological manifold:

**Definition 1** (Topological Manifold)**.** *A topological space $M$ is said to be a* **topological manifold** *of dimension $n$ if it satisfies the following three properties:*

- *(i) $M$ is a Hausdorff space: Given any two points $p, q \in M$ there exist disjoint open subsets $U, V \subset M$ such that $p \in U$ and $q \in V$.*
- *(ii) $M$ is second countable: There exists a countable basis for the topology of $M$.*
- *(iii) $M$ is locally Euclidean of dimension $n$: Every point of $M$ has a neighbourhood that is homeomorphic to an open subset of $\mathbb{R}^n$.*

In the definition above, property (*iii*) is equivalent to stating that for each $p \in M$ we can find an open set $U \subset M$ containing $p$, an open set $\tilde{U} \subset \mathbb{R}^n$, and a homeomorphism $\varphi : U \to \tilde{U}$. This naturally leads to the definition of a coordinate chart:

**Definition 2** (Coordinate Chart)**.** *A* **coordinate chart** *on a manifold $M$ of dimension $n$ is a pair $(U, \varphi)$, where $U$ is an open subset of $M$ and $\varphi : U \to \tilde{U}$ is a homeomorphism from $U$ to an open subset $\tilde{U} = \varphi(U) \subset \mathbb{R}^n$.*

By the discussion of property (*iii*) above, each point $p \in M$ is contained in the domain of some chart $(U, \varphi)$. We will call a collection of coordinate charts whose domain covers $M$ an atlas. We would like to further examine the overlap of coordinate charts in a given atlas. In order to accomplish this, we will use the following definition:

**Definition 3** (Transition Map)**.** *Let $M$ be an $n$-dimensional topological manifold. If $(U, \varphi)$ and $(V, \psi)$ are two charts such that $U \cap V \neq \emptyset$, then the composition map $\psi \circ \varphi^{-1} : \varphi(U \cap V) \to \psi(U \cap V)$ is called the* **transition map** *from $\varphi$ to $\psi$.*

The transition map as defined above is a composition of homeomorphisms and is therefore a homeomorphism itself. Two charts $(U, \varphi)$ and $(V, \psi)$ are said to be smoothly compatible if either $U \cap V = \emptyset$ or the transition map $\psi \circ \varphi^{-1}$ is a diffeomorphism. This allows us to define a smooth atlas which is an atlas $\mathcal{A}$ in which any two charts are smoothly compatible with each other. We say that a smooth atlas is maximal if it is not contained in any strictly larger smooth atlas. This leads us to the main definition of this section:

**Definition 4** (Differentiable Manifold)**.** *A* **differentiable manifold** *is a pair $(M, \mathcal{A})$ where $M$ is a topological manifold of dimension $n$ and $\mathcal{A}$ is a maximal smooth atlas on $M$.*

For the remainder of this chapter we will focus our attention on differentiable manifolds as this particular type of manifold will allow us to define and analyze intrinsic differential structures. We proceed by giving an example of a differentiable manifold.

**Sphere -** $\mathbb{S}^n$ Let $\mathbb{S}^n = \{\mathbf{x} := (x_1, \ldots, x_{n+1}) \in \mathbb{R}^{n+1} : \|\mathbf{x}\| = 1\}$ be the standard $n$-dimensional sphere. Set

$$U = \mathbb{S}^n \setminus \{(0, \ldots, 0, 1)\}$$
$$V = \mathbb{S}^n \setminus \{(0, \ldots, 0, -1)\}$$

and define the stereographic projections, $\varphi : U \to \mathbb{R}^n$ and $\psi : V \to \mathbb{R}^n$, by

$$\varphi(\mathbf{x}) := \frac{1}{1 - x_{n+1}}(x_1, \ldots, x_n)$$
$$\psi(\mathbf{x}) := \frac{1}{1 + x_{n+1}}(x_1, \ldots, x_n).$$

we will show that the coordinate systems $(U, \varphi)$ and $(V, \psi)$ are compatible, thereby demonstrating that $\mathbb{S}^n$ is indeed a differentiable manifold.

*Proof.* In order to verify that $(U, \varphi)$ and $(V, \psi)$ are compatible, we must check that $\varphi \circ \psi^{-1}$ and $\psi \circ \varphi^{-1}$ are both smooth functions. We will begin by showing that $\varphi$ and $\psi$ are surjective and injective and therefore bijective. This will imply that both $\varphi \circ \psi^{-1}$ and $\psi \circ \varphi^{-1}$ are functions.

Let $x = (x_1, \ldots, x_n)$ be a point in the plane $x_{n+1} = 0$. Now, consider the point given by

$$(X_1, \ldots, X_{n+1}) = \left( \frac{2x_1}{1 + \sum_{i=1}^n x_i^2}, \ldots, \frac{2x_n}{1 + \sum_{i=1}^n x_i^2}, \frac{-1 + \sum_{i=1}^n x_i^2}{1 + \sum_{i=1}^n x_i^2} \right)$$

which lies in $U$. Observe that $\varphi((X_1, \ldots, X_{n+1})) = (x_1, \ldots, x_n)$:

$$\begin{aligned} \varphi((X_1, \ldots, X_{n+1})) &= \left( \frac{2x_1}{1 + \sum_{i=1}^n x_i^2} \Big/ 1 - \left( \frac{-1 + \sum_{i=1}^n x_i^2}{1 + \sum_{i=1}^n x_i^2} \right), \ldots, \frac{2x_n}{1 + \sum_{i=1}^n x_i^2} \Big/ 1 - \left( \frac{-1 + \sum_{i=1}^n x_i^2}{1 + \sum_{i=1}^n x_i^2} \right) \right) \\ &= (x_1, \ldots, x_n). \end{aligned}$$

Hence, for every point $(x_1, \ldots, x_n)$ in the plane $x_{n+1} = 0$, there exists a point on the sphere $(X_1, \ldots, X_n) \in U$ such that $\varphi((X_1, \ldots, X_{n+1})) = (x_1, \ldots, x_n)$. This shows that $\varphi : U \to \mathbb{R}^n$ is surjective.

A similar argument can be made for $\psi : V \to \mathbb{R}^n$, where the point $Y \in V$ corresponding to $y = (y_1, \ldots, y_n)$ is given by:

$$(Y_1, \ldots, Y_{n+1}) = \left( \frac{2y_1}{1 + \sum_{i=1}^n y_i^2}, \ldots, \frac{2y_n}{1 + \sum_{i=1}^n y_i^2}, \frac{1 - \sum_{i=1}^n y_i^2}{1 + \sum_{i=1}^n y_i^2} \right)$$

Hence, both $\varphi$ and $\psi$ are surjective. We will now proceed by showing that both mappings are also injective. We will do this by showing that $\varphi$ and $\psi$ are left-invertible. As above, we will deal first with $\varphi$. Consider the mapping $\Phi : \varphi(U) \to U$ such that

$$\Phi(\mathbf{x}) = \left( \frac{2x_1}{1 + \sum_{i=1}^n x_i^2}, \ldots, \frac{2x_n}{1 + \sum_{i=1}^n x_i^2}, \frac{-1 + \sum_{i=1}^n x_i^2}{1 + \sum_{i=1}^n x_i^2} \right),$$

where $\mathbf{x} = (x_1, \ldots, x_n) \in \varphi(U) \subset \mathbb{R}^n$. Now suppose we have a point $X = (X_1, \ldots, X_{n+1}) \in U$, so that $\varphi(X)$ is given by

$$\varphi(X) = \left( \frac{X_1}{1 - X_{n+1}}, \ldots, \frac{X_n}{1 - X_{n+1}} \right).$$

Now the composition $\Phi \circ \varphi(X)$ gives us:

$$\begin{aligned} \Phi \circ \varphi(X) &= \left( \frac{X_1}{1 - X_{n+1}} \Bigg/ 1 + \sum_{i=1}^{n} \left( \frac{X_i}{1 - X_{n+1}} \right)^2, \ldots, -1 + \sum_{i=1}^{n} \left( \frac{X_i}{1 - X_{n+1}} \right)^2 \Bigg/ 1 + \sum_{i=1}^{n} \left( \frac{X_i}{1 - X_{n+1}} \right)^2 \right) \\ &= (X_1, \ldots, X_{n+1}). \end{aligned}$$

Hence, $\Phi \circ \varphi(X)$ is the identity function on $U$, and it follows that $\varphi$ is injective. Clearly a similar argument can be made to show that $\psi$ is also injective, where we will let $\Psi$ denote the left-inverse. Since $\varphi$ and $\psi$ are surjective and injective, they are both bijective. Moreover, $\Phi$ and $\Psi$ are the inverses of $\varphi$ and $\psi$ respectively. That is, $\Phi = \varphi^{-1}$ and $\Psi = \psi^{-1}$. It follows that both of the transition maps given below are bijective:

$$\begin{aligned} \psi \circ \varphi^{-1} &: \varphi(U \cap V) \to \psi(U \cap V) \\ \varphi \circ \psi^{-1} &: \psi(U \cap V) \to \varphi(U \cap V), \end{aligned}$$

where $\varphi(U \cap V) \subset \mathbb{R}^n$ and $\psi(U \cap V) \subset \mathbb{R}^n$. Now we will proceed by checking that $\psi \circ \varphi^{-1}$ and $\varphi \circ \psi^{-1}$ are indeed smooth. To do so, we explicitly write the function compositions. One can check that the first function composition is given by:

$$\psi \circ \varphi^{-1}(X) = \left( \frac{x_1}{\sum_{i=1}^{n} x_i^2}, \ldots, \frac{x_n}{\sum_{i=1}^{n} x_i^2} \right),$$

where the $x_j$ are given by:

$$x_j = \frac{X_j}{1 - X_{n+1}}.$$

It is clear that this mapping is indeed smooth. A similar mapping may also be constructed for $\varphi \circ \psi^{-1}$ which will also be smooth. This verifies that the coordinate charts $(U, \phi)$ and $(V, \psi)$ are smoothly compatible, and that $\mathbb{S}^n$ is therefore a differentiable manifold. □

In the section that follows we will turn our attention to defining explicit smooth structures on manifolds. In particular, we will construct a 'metric tensor' which is a differential structure on a smooth manifold that allows us to measure lengths and distances. This mathematical object will play a key role in our study of PDEs on surfaces for the remainder of the thesis.

## 1.1 Geometric Properties of Smooth Manifolds

We will now turn our attention to understanding smooth manifolds from a differential viewpoint. This is necessary as our ultimate goal is to define and solve PDEs on such surfaces. We will take the classical approach of constructing partitions of unity on a given smooth manifold $M$. We will then use the partition of unity construction to define an inner product on the tangent space of the manifold at a given point $p \in M$. This ultimately leads to the construction of a metric tensor which is a symmetric positive definite bilinear form that varies smoothly on the tangent bundle of the given manifold. As we will see, such a tensor can be constructed for any smooth manifold, though it is in general not unique. In the sections that follow, we will use the metric tensor to develop a notion of PDEs on manifolds. The metric will also play a significant role in the numerical computations that we perform which lie at the heart of the thesis. We will begin by giving a definition of a partition of unity.

**Definition 5** (Partition of Unity)**.** *A Partition of Unity on a manifold is a collection* $\{f_i\}_{i\in I}$ *of* $C^\infty$ *functions on* $M$ *such that*

*(i) The* $f_i$ *obey:* $0 \leq f_i \leq 1$

*(ii)* $\{supp(f_i)\}_{i\in I}$ *is locally finite*

*(iii)* $\sum_{i\in I} f_i(p) = 1$*, for all* $p \in M$*.*

We say that a partition of unity is subordinate to an open covering $\{A_\alpha\}$ of $M$ if for each $i \in I$, there exists $\alpha(i)$ such that $\text{supp}(f_i) \subset A_{\alpha(i)}$. We now prove a theorem regarding the existence of partitions of unity on smooth manifolds.

**Theorem 1.** *Let* $M$ *be a smooth manifold and let* $\{A_\alpha\}$ *be an open covering of* $M$*. There is a partition of unity subordinate to* $\{A_\alpha\}$*.*

*Proof.* We begin by first refining the covering. Since $M$ is second countable, then there is a countable base, $\{\theta_i\}$, such that each $\bar{\theta_i}$ is compact. Define a nested sequence $K_1, K_2, \ldots$ where $K_1 = \bar{\theta}_1$. Let $r_1$ be the smallest integer such that $\bar{\theta}_1 \subset \cup_{j=1}^{r_1}\theta_j$.

Now, we have

$$K_2 = \overline{\left(\cup_{j=1}^{r_1}\theta_j\right)} = \cup_{j=1}^{r_1}\bar{\theta}_j,$$

and furthermore $K_{i+1}$ can be written as:

$$K_{i+1} = \bar{\theta}_1 \cup \ldots \cup \bar{\theta}_{r_i}.$$

Now given $p \in K_{i+1} - \overset{\circ}{\mathrm{K}}_i$ for $i \in \mathbb{N}$, where $\overset{\circ}{\mathrm{K}}_i$ denotes the interior of $K_i$, we can choose a chart $(U_{p_\alpha}, \varphi_{p_\alpha})$ about $p$ such that $\varphi_{p_\alpha}(p) = 0$ and $\varphi_{p_\alpha}(U_{p_\alpha}) = B_3^n(0)$. Ultimately, we want to find $U_{p_\alpha}$ such that

$$U_{p_\alpha} \subset (\overset{\circ}{\mathrm{K}}_{i+2} - K_{i-1}) \cap A_\alpha.$$

We will do this by taking a chart contained in the right hand side of the above expression and intersect it with the right hand side and then we will restrict $\varphi$ to this open set. Accordingly, define

$$V_{p_\alpha} = \varphi_{p_\alpha}^{-1}(B_1^n(0)),$$

which can be done for all $p \in K_{i+1} - \overset{\circ}{\mathrm{K}}_i$, giving us a family of open sets $\{V_{p_\alpha}\}$. Since $K_{i+1} - \overset{\circ}{\mathrm{K}}_i$ is compact, it can be covered with a finite subset of $\{V_{p_\alpha}\}$, say $\{V_{i,k}\}_{k=1}^{n_i}$. From this we can get a countable cover, say $\{V_j\}_{j=1}^{\infty}$ with corresponding charts $(U_j, \varphi_j)$. Under this construction $\{V_j\}_{j=1}^{\infty}$ is locally finite with $V_j \subset A_\alpha$ for some $\alpha$. □

We will use the existence of a partition of unity on a smooth manifold to construct a metric tensor which is a smooth assignment of an inner product on the tangent space, $T_pM$, at each point $p \in M$. The formal definition of a metric tensor is given below:

**Definition 6** (Metric Tensor)**.** *A Riemmanian metric $g$ on a manifold $M$ is a $(0,2)$-tensor field on $M$ that is a family of symmetric and positive definite inner products*

$$g_p : T_pM \times T_pM \to \mathbb{R}, p \in M$$

*such that for all differentiable vector fields $X, Y$ on $M$,*

$$p \to g_p(X(p), Y(p))$$

*defines a smooth function $M \to \mathbb{R}$.*

We will now demonstrate that all smooth manifolds admit a Riemannian metric.

**Theorem 2.** *Every smooth manifold admits a Riemannian metric.*

*Proof.* Let $\{U_i, \varphi_i\}_{i \in I}$ be an atlas for $M$. We can always choose a Riemannian metric on a coordinate neighborhood by setting:

$$g_i = \varphi_i^* g_{\text{Euc}},$$

where $g_{\text{Euc}}$ is the typical euclidean metric under the pullback $\varphi_i^*$. We choose a partition of unity $\{f_i\}$ subordinate to $\{U_i\}$ and let

$$g = \sum_i f_i g_i.$$

We will proceed by verifying that this defines a Riemannian metric. In doing so, the only non-trivial property that we must check is that $g$ is positive definite. To show that it is positive definite, we observe that for all $p \in M$, there exists $j \in \mathbb{N}$ such that $f_j(p) > 0$ and if $V_{x_0} \in T_pM$ then

$$\begin{aligned} g_p(v, v) &= \sum_i f_i(p) g_i(v, v) \\ &\geq f_j(p) g_i(v, v) \\ &> 0. \end{aligned}$$

It follows that $g$ is positive definite. Therefore, $g$ is a metric on $M$. □

For our purposes, we will focus our attention specifically on manifolds that posses a Riemannian metric. For completeness, we end this section with the definition of such a structure, which we call a Riemannian manifold.

**Definition 7** (Riemannian Manifold)**.** *A Riemannian manifold is a smooth manifold equipped with a metric tensor $g$. A given Riemannian manifold is typically denoted $(M, g)$.*

For the remainder of the thesis, we will assume that the manifolds we are dealing with are Riemannian unless otherwise stated.

## 1.2 Construction of the Laplace-Beltrami Operator on Riemannian Manifolds

We will now proceed to present the mathematical ideas needed to construct the Laplace-Beltrami operator, which is a geometric operator on a Riemannian manifold that is analogous

to the Laplace operator in Euclidean space. In order to construct the Laplace-Beltrami operator, we will first briefly present some of the basic ideas of differential forms and Hodge theory needed to study differential structure on Riemannian manifolds. The discussion that follows is not meant to be exhaustive, but rather it is meant to be a starting point from which one may understand some of the mathematics underlying the solution of PDEs on manifolds.

**Definition 8.** *(Wedge Product) Let $\omega \in \Lambda^k(V)$ and $\eta \in \Lambda^l(V)$, we define the* **wedge product** *to be the alternating $(k+l)$-tensor*

$$\omega \wedge \eta = \frac{(k+l)!}{k!\, l!} \operatorname{Alt}(\omega \otimes \eta).$$

Notice that for a given manifold, $\Lambda^k(T_p^*M)$ and $\Lambda^{n-k}(T_p^*M)$ have the same dimension, where $0 \leq k \leq n$. This follows from the fact that $\dim(\Lambda^k(V)) = \binom{n}{k}$ and the simple identity $\binom{n}{k} = \binom{n}{n-k}$.

For a given oriented Riemannian manifold, we may multiply by the volume form $dV_g = \sqrt{\det(g_{ij})} dx^1 \wedge \ldots \wedge dx^n$ to get the linear map $* : C^\infty(M) \to \Lambda^n(M)$:

$$*f = f dV_g.$$

It can be checked that this induces a linear isomorphism $* : C^\infty(M) \cong \Lambda^n(M)$. Moreover, this definition can be naturally extended to induce a further isomorphism $* : \Lambda^k(T_p^*M) \cong \Lambda^{n-k}(T_p^*M)$ given by

$$*(\theta^1 \wedge \ldots \wedge \theta^k) = \theta^{k+1} \wedge \ldots \wedge \theta^n,$$

where $\theta^1, \ldots, \theta^k, \theta^{k+1}, \ldots, \theta^n$ are an arbitrary positively oriented orthonormal basis for $T_p^*M$. This is known as the Hodge-star operator, and it is quite useful in constructing differential operators on compact oriented Rieammanian manifolds. We now give several important properties of the Hodge-star operator.

**Proposition 1.** *Let $\omega, \eta \in \mathcal{A}^k(M)$ be $k$-forms and let $f, g \in C^\infty(M)$ be functions on $(M, g)$, then the following three properties hold:*

*(i)* $*(f\omega + g\eta) = f * \omega + g * \eta$

*(ii)* $** \omega = (-1)^{k(n-k)}\omega$

*(iii)* $\omega \wedge *\eta = \langle \omega, \eta \rangle_g dV_g$.

*Proof.* It will suffice to prove the desired results for a general point $p \in M$.

(i) The property follows directly from the linearity of the Hodge star operator $*$.

(ii) Let $\theta_1, \ldots, \theta_n$ be a positive orthonormal basis for $T_p^*M$. We may assume that $\omega = \theta_1 \wedge \ldots \wedge \theta_k$, so that $*\omega_p = \theta_{k+1} \wedge \ldots \wedge \theta_n$. By applying the Hodge star operator once more, we obtain

$$** \omega_p = (-1)^{k(n-k)} \omega_p,$$

which is the desired result.

(iii) Since each term is linear in $\eta$, we assume in the argument above that $\eta_p = \theta_{i_1} \wedge \ldots \theta_{i_k}$. In this case, we have

$$*\eta_p = \operatorname{sgn}(I, J) \theta_{j_1} \wedge \ldots \wedge \theta_{j_{n-k}}.$$

The only time when $\omega_p \wedge *\eta_p \neq 0$ is when $\{i_1, \ldots, i_k\} = \{1, \ldots, k\}$, and then we have

$$\omega_p \wedge *\eta_p = \operatorname{sgn}(I) \theta_1 \wedge \ldots \wedge \ldots \wedge \theta_n,$$

where $\operatorname{sgn}(I)$ is the sign of the permutation $i_1, \ldots, i_k$.

On the other hand, we have that $\langle \omega_p, \eta_p \rangle_g \neq 0$ only if $\{i_1, \ldots, \imath_k\} = \{1, \ldots, k\}$, in which case we have $\langle \omega_p, \eta_p \rangle_g = \operatorname{sgn}(I)$. This proves the desired result. □

We will now proceed to define the Laplace-Beltrami operator by means of the the differential map $d : \Lambda^k(T_p^*M) \to \Lambda^{k+1}(T_p^*M)$ and the Hodge star operator. For this purpose, we define a linear operator

$$d^* = (-1)^k *^{-1} d* = (-1)^{n(k+1)+1} * d * .$$

This leads directly to the definition of the Laplace-Beltrami operator:

**Definition 9** (Laplace-Beltrami)**.** *For a given Riemannian manifold* $(M, g)$*, the* **Laplace-Beltrami** *operator is defined by:*

$$\Delta = dd^* + d^*d.$$

It can be shown that the above definition of the Laplace-Beltrami operator agrees with the Laplacian $\Delta_g = -\operatorname{Div}(\operatorname{Grad}(u))$ for smooth functions $u$ on $(M, g)$, for more details and a short proof of this fact, see [J.Lee]. In the next section, we will further investigate the Laplace-Beltrami operator.

## 1.3 The Laplace-Beltrami Operator in Local Coordinates

In this section, we give a brief derivation of the Laplace-Beltrami operator stated in a local coordinate system for a given manifold $(M, g)$. The derivation is similar in nature to the case where $M = \mathbb{R}^n$. Now, let $\varphi : M \to \mathbb{R}$ and proceed as follows:

$$\begin{aligned}
\int \Delta u \cdot \varphi \sqrt{|g|} dx^1 \wedge \ldots \wedge dx^n &= (\Delta u, \varphi) \\
&= (du, d\varphi) \\
&= \int \langle du, d\varphi \rangle \sqrt{|g|} dx^1 \wedge \ldots \wedge dx^n \\
&= \int g^{ij} \frac{\partial u}{\partial x^i} \frac{\partial \varphi}{\partial x^j} \sqrt{|g|} dx^1 \ldots dx^n \\
&= -\int \frac{1}{\sqrt{|g|}} \frac{\partial}{\partial x^j} \left( \sqrt{|g|} g^{ij} \frac{\partial u}{\partial x^i} \right) \varphi \sqrt{|g|} dx^1 \ldots dx^n,
\end{aligned}$$

which holds for all $\varphi \in C_0^\infty(M, \mathbb{R})$ and where $|g| := \det(g_{ij})$. The final integral gives us our desired expression for the Laplacian in local coordinates, namely:

$$\Delta_g u = -\frac{1}{\sqrt{|g|}} \frac{\partial}{\partial x^j} \left( \sqrt{|g|} g^{ij} \frac{\partial u}{\partial x^i} \right).$$

In the above calculation, the Einstein summation convention was used.

### 1.3.1 Example: Derivation of the Spherical Laplacian

In order to demonstrate the utility of the coordinate representation of the Laplace-Beltrami operator, we will proceed to derive the formula for the spherical Laplacian. We start with the parametric representation of the spherical coordinate system:

$$\begin{cases} x &= r \sin\theta \cos\varphi \\ y &= r \sin\theta \sin\varphi \\ z &= r \cos\theta \end{cases}.$$

Recall that $g_{ij} = [(\partial u/\partial x^i) \cdot (\partial u/\partial x_j)]_{ij}$, so we will proceed by computing the $\partial u/\partial x^i$:

$$\begin{aligned}
\frac{\partial u}{\partial r} &= (\sin\theta\cos\varphi, \sin\theta\sin\varphi, \cos\theta) \\
\frac{\partial u}{\partial \theta} &= (r\cos\theta\cos\varphi, \cos\theta\sin\varphi, -r\sin\theta) \\
\frac{\partial u}{\partial \varphi} &= (-r\sin\theta\sin\varphi, r\sin\theta\cos\varphi, 0).
\end{aligned}$$

Now, we will compute the terms along the trace. Starting with $(\partial u/\partial r) \cdot (\partial u/\partial r)$ we have:

$$\begin{aligned}
\frac{\partial u}{\partial r}\frac{\partial u}{\partial r} &= (\sin\theta\cos\varphi)^2 + (\sin\theta\sin\varphi)^2 + \cos^2\theta \\
&= \sin^2\theta\cos^2\varphi + \sin^2\theta\sin^2\varphi + \cos^2\theta \\
&= \sin^2\theta(\cos^2\varphi + \sin^2\varphi) + \cos^2\theta \\
&= \sin^2\theta + \cos^2\theta \\
&= 1.
\end{aligned}$$

The term $(\partial u/\partial\theta) \cdot (\partial u/\partial\theta)$ is given by:

$$\begin{aligned}
\frac{\partial u}{\partial \theta}\frac{\partial u}{\partial \theta} &= (r\cos\theta\cos\varphi)^2 + (r\cos\theta\sin\varphi)^2 + (-r\sin\theta)^2 \\
&= r^2\cos^2\theta\cos^2\varphi + r^2\cos^2\theta\sin^2\varphi + r^2\sin^2\theta \\
&= r^2(\cos^2\theta(\cos^2\varphi + \sin^2\varphi) + \sin^2\theta) \\
&= r^2(\cos^2\theta + \sin^2\theta) \\
&= r^2.
\end{aligned}$$

Finally, the term $(\partial u/\partial\varphi) \cdot (\partial u/\partial\varphi)$ is given by:

$$\begin{aligned}
\frac{\partial u}{\partial \varphi}\frac{\partial u}{\partial \varphi} &= (r\sin\theta\sin\varphi)^2 + (r\sin\theta\cos\varphi)^2 + 0 \\
&= r^2\sin^2\theta\sin^2\varphi + r^2\sin^2\theta\cos^2\varphi \\
&= r^2\sin^2\theta(\sin^2\varphi + r^2\cos^2\varphi) \\
&= r^2\sin^2\theta.
\end{aligned}$$

One may check that the non-trace terms, i.e., $(\partial u/\partial x^i) \cdot (\partial u/\partial x_j)$ for $i \neq j$, evaluate to zero. Hence, we may represent the metric tensor in matrix form as:

$$g_{ij} = \begin{bmatrix} 1 & 0 & 0 \\ 0 & r^2 & 0 \\ 0 & 0 & r^2 \sin^2 \theta \end{bmatrix},$$

and $g^{ij}$ is given by:

$$g^{ij} = \begin{bmatrix} 1 & 0 & 0 \\ 0 & 1/r^2 & 0 \\ 0 & 0 & 1/(r^2 \sin^2 \theta) \end{bmatrix}.$$

At this point we have computed the metric tensor for a spherical coordinate system and we may now proceed by means of the coordinate representation for the Laplace-Beltrami operator:

$$\Delta_g u = -\frac{1}{\sqrt{|g|}} \frac{\partial}{\partial x^j} \left( \sqrt{|g|} g^{ij} \frac{\partial u}{\partial x^i} \right).$$

We will do this for each of the trace $x^i$ terms then some over the resulting expressions. The three trace terms corresponding to $x^1 = r, x^2 = \theta$, and $x^3 = \varphi$ are given by:

$$\begin{aligned} \Delta_{g_{11}} u &= -\frac{1}{r^2 \sin \theta} \frac{\partial}{\partial r} \left( r^2 \sin \theta \cdot (1) \cdot \frac{\partial u}{\partial r} \right) \\ \Delta_{g_{22}} u &= -\frac{1}{r^2 \sin \theta} \frac{\partial}{\partial \theta} \left( r^2 \sin \theta \cdot \left( \frac{1}{r^2} \right) \cdot \frac{\partial u}{\partial \theta} \right) \\ \Delta_{g_{33}} u &= -\frac{1}{r^2 \sin \theta} \frac{\partial}{\partial \varphi} \left( r^2 \sin \theta \cdot \left( \frac{1}{r^2 \sin \theta} \right) \cdot \frac{\partial u}{\partial \varphi} \right). \end{aligned}$$

Now, summing over the $\Delta_{g_{ii}}(\cdot)$ terms gives us the Laplace-Beltrami operator for the sphere, which we immediately recognize as the spherical Laplacian:

$$\Delta u = \frac{1}{r^2} \frac{\partial}{\partial r} \left( r^2 \frac{\partial u}{\partial r} \right) + \frac{1}{r^2 \sin \theta} \frac{\partial}{\partial \theta} \left( \sin \theta \frac{\partial u}{\partial \theta} \right) + \frac{1}{r^2 \sin^2 \theta} \frac{\partial^2 u}{\partial \varphi^2}.$$

At this point, we have an expression for the Laplacian in spherical coordinates, however, it may not be clear how this expression can be used to practically evolve a PDE involving the Laplacian on a spherically symmetric manifold. For this reason, we are typically interested in studying harmonic functions on the sphere (or more generally on a given manifold $M$). This will give us a better sense of how to evolve equations involving Laplace-Beltrami operators.

# Chapter 2

# The Closest Point Method

In recent years, the problem of evolving PDEs on manifolds embedded in $\mathbb{R}^n$ has become a topic of much interest. As we saw in the previous section, it can be quite difficult to pose and subsequently construct fundamental solutions for these types of PDEs in the general. Moreover, several numerical techniques have been developed to deal with precisely this issue. Three main approaches to have arisen which we will briefly explain below:

1. **Analytic Methods**: The classical approach to evolving PDEs on Manifolds is to compute geometric properties directly from the metric tensor $g_{ij}$. The derivations of metric tensors and Laplace-Beltrami operators that we presented in the previous section is an example of how to apply the theory of this approach to perform actual calculations. This approach has provided much information about the existence of solutions of certain types of PDEs as well as the spectra of differential operators on manifolds. Several asymptotic estimates have also been produced with this method. However, as we saw in the previous section, even for some basic manifolds such as the genus 1 torus, it can be quite difficult to actually perform calculations analytically using this approach.

2. **Parameterization Methods**: Another technique that is similar in nature to the analytic approach is to define a parametrization $P : M \to \mathbb{R}^n$ of the given manifold. The corresponding PDE system is then mapped to $\mathbb{R}^n$ where standard numerical techniques may be applied, and then the resulting solution is mapped back to the original manifold $M$ using the inverse mapping of the parametrization. Clearly, there

are also some problems that arise with this method. Firstly, it is in general a non-trivial procedure to find a parametrization of a given manifold, and this step can often times be more difficult than solving the actual PDE itself. In addition many surfaces cannot actually be parameterized, and parametrizations on other surfaces may lead to artificial singularities.

3. **Finite Element Method**: Perhaps the most ubiquitous method in applied mathematics for solving PDEs involving in-surface flows is the finite element method. Created in the 1940s by Alexander Hrennikoff and Richard Courant, the method relies approximating the surface in questions via a triangulation. Following the process of triangulation, a weak formulation of the given PDE along with its boundary conditions are posed on each triangulated face. The Hilbert space in which the solution of the weak-formulation lives is then replaced with a finite dimensional subspace. Once a basis is selected for the finite dimensional subspace, a discretization and hence a matrix formulation for the given problem is obtained and the corresponding system is solved via computer. Although the finite element method is incredibly versatile in the nature of problems that it can solve, it is often non-trivial to construct a triangulation of the underlying domain. This is especially true of the given surface in question exhibits a highly complicated geometry.

4. **Embedding Methods**: In the late 1990s several mathematicians also worked on developing methods for solving PDEs on $n$-dimensional manifolds based on embedding the differential structures into a narrow region around the manifold in $\mathbb{R}^{n+1}$. Although this technique is quite effective for many problems, it leads to the imposition of artificial boundary conditions in $\mathbb{R}^{n+1}$ which do not necessarily have physical meaning. In addition, this approach requires the re-initialization of level set functions for every time step of the method.

We will now proceed to construct the Closest Point Method - a numerical method for effectively dealing with differential structures on manifolds. The method is based on two geometric principals, the first of which states that a function on a surface which is constant in the normal direction will only vary along paths that are intrinsic to the surface. The second principle states that a flux that is directed along a surface can only spread along paths that are intrinsic to the surface. Using these two principles, a wide class of PDEs can be solved on manifolds that are quite general. We will make these notions precise in the

discussion that follows. We begin by giving a precise definition of what is meant by "closest point":

**Definition 10** (Closest Point Function)**.** *Let $x \in \mathbb{R}^n$ and let $M \subset \mathbb{R}^n$. By the closest point we mean the function $CP(x)$ such that the following holds:*

$$CP(x) := x - (\nabla d(x)) \cdot d(x),$$

*where*

$$d(x, M) := \inf_{y \in M} |x - y|.$$

Note that if $M$ is a co-dimension one embedding with respect to $\mathbb{R}^n$, then the vector extending from the surface to the closest point will be normal to the surface. Now, two fundamental geometric properties can be stated as follows:

1. If $u$ is a function defined on the surface, $u(CP)$ is constant along directions normal to the surface, so that the first principle implies:

$$\nabla u(CP) = \nabla_g u.$$

2. The gradient given by $\nabla u(CP)$ is always tangent to the level sets of the distance function. By the second principle, this implies the following:

$$\nabla \cdot (\nabla u(CP)) = \nabla_g \cdot (\nabla_g u).$$

For further reference on why these principles hold, see [18]. Together these two principles can be used to solve a wide-variety of PDEs on surfaces. As an example, we solve a pattern formation PDE intrinsic to the surface of a sphere. The results for several different time steps are shown below.

## 2.1 Existence of the Closest Point Function for Compact Smooth Manifolds

So far we have considered surfaces that have an obvious embedding in $\mathbb{R}^n$ for some $n \in \mathbb{N}$. As a consequence of the particular embedding that we chose, we were able to construct a corresponding closest point function for points in the ambient space. (The Closest Point Method as we have constructed it is an extrinsic geometric method).

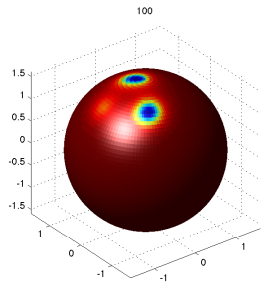


(a) $i = 100$

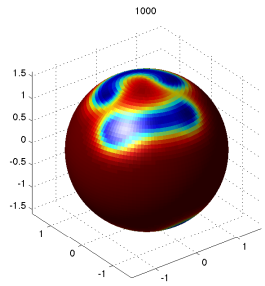


(b) $i = 1000$

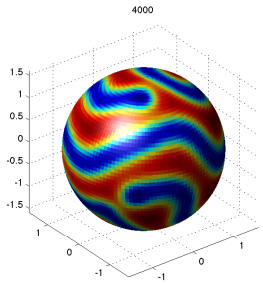


(c) $i = 4000$

Figure 2.1: Above are three different plots of a pattern formation PDE on the surface of a sphere.

In general, we may be given an abstract smooth manifold $(M, g)$ which does not necessarily have an obvious embedding in Euclidean space. In fact the question of whether or not such an embedding exists was a classical problem in manifold theory until it was affirmatively answered in the 1930s by Hassler Whitney. For the definition of an embedding and full proof of the Whitney embedding theorem, see [10]. The Whitney embedding theorem states that any smooth $n$-manifold can be smoothly embedded in $\mathbb{R}^{2n+1}$ space. In fact Whitney developed a stronger form of the embedding theorem which guarantees a smooth embedding in $\mathbb{R}^{2n}$ and an immersion in $\mathbb{R}^{2n-1}$. We will present a weak form of the embedding theorem for compact smooth manifolds and show that as a consequence the closest point method can be applied to this class of manifolds.

**Theorem 3** (Whitney)**.** *Let $M$ be a compact manifold of dimension $n$, then there exists an embedding $f : M \to \mathbb{R}^N$ for some integer $N \geq n$.*

*Proof.* Since $M$ is compact, it follows from the proof for the existence of partitions of unity

that there exist charts $\{(U_1, \varphi_1), \ldots, (U_k, \varphi_k)\}$ with $M = U_1 \cup \ldots \cup U_k$ and there exist $U_i' \subset U_i$ that also cover $M$ and smooth functions $f : M \to [0, 1]$ such that $\text{supp}(f_i) \subset U_i$ and $f_i = 1$ on $U_i'$.

Now define $F : M \to \mathbb{R}^N$, with $N = nk + k$, by:

$$F = (f_1\varphi_1, \ldots, f_k\varphi_k, f_1, \ldots, f_k).$$

We will now show that $F$ is an immersion by showing that the differential $\text{rank}(dF_p) = n$, where $n$ is the dimension of the manifold. To show this, consider $p \in M$ for which we know that $p \in U_i'$ for some $i$. The Jacobian with respect to the chart $(U_i, \varphi_i = (x^1, \ldots, x^n))$ is given by the $N \times n$ matrix:

$$J = \left[\frac{\partial F^i}{\partial x^j}\right],$$

where $1 \leq i \leq N$ and $1 \leq j \leq n$. By noting that this matrix contains the $n \times n$ block $[\partial x^i / \partial x^j] = I_{n\times n}$, we conclude that $dF_p$ has rank $n$.

To see that $F$ is injective, suppose that $F(p) = F(q)$. We know that there exists an $i$ such that $p \in U_i'$. Moreover, by the hypothesis $F(p) = F(q)$, it follows that $f_i(p) = 1$ implies $f_i(q) = 1$ and hence $q \in U_i'$. Also, we have

$$f_i(p)\varphi_i(p) = \varphi_i(p),$$
$$f_i(p)\varphi_i(q) = \varphi_i(q),$$

and since $\varphi_i$ is a bijection, it follows that $p = q$.

Therefore, we conclude that $F$ is an injective immersion of a compact manifold which implies that it is an embedding. □

The benefit of this particular construction is that we are given an explicit embedding $F : M \to \mathbb{R}^{nk+k}$. Given this embedding we may apply the closest point operator to an arbitrary point $x \in \mathbb{R}^{nk+k}$ with respect to $F$. In particular, this gives us

$$CP(x) := x - (\nabla d(x, F)) \cdot d(x, F),$$

where as above

$$d(x, F) := \inf_{y \in F} |x - y|.$$

This directly gives us the existence of the closest point function for compact smooth manifolds, which we formally state as a corollary of the embedding theorem presented above.

**Corollary 1.** *Given an arbitrary compact smooth manifold $M$, there exists a closest point function for $x \in \mathbb{R}^{nk+k}$ with respect to the embedding*

$$F = (f_1\varphi_1, \ldots, f_k\varphi_k, f_1, \ldots, f_k).$$

It should be noted that this result is primarily for theoretical purposes as the given embedding is far from optimal. For example, under this embedding the typical 2-sphere is embedded in $\mathbb{R}^6$ instead of the typical $\mathbb{R}^3$. The power of this result is that it demonstrates that the closest point method can be applied to a manifold so long as it is smooth and compact.

## 2.2 Numerical Implementation of the Closest Point Method

At this point we turn our attention to translating the ideas presented thus far into a numerical method for solving PDEs on surfaces. The discussion follows from the steps presented in [18] The method is initialized by computing several quantities.

1. **Closest Point Representation**: Compute the closest point representation of the surface with respect to ambient space $\mathbb{R}^n$ that it is embedded in. In practice, this is typically done by solving the minimization problem:

   $$CP(x) := x - (\nabla d(x, M)) \cdot d(x, M),$$

   with

   $$d(x, M) := \inf_{y \in M} |x - y|.$$

   This is performed for each grid node in the computational domain which is a subset of $\mathbb{R}^n$.

2. **Banding**: Compute the bandwidth for the given problem using the formula:

   $$\lambda = \sqrt{(n-1)\left(\frac{p+1}{2}\right)^2 + \left(1 + \frac{p+1}{2}\right)^2}\Delta x,$$

where $p$ is the degree of the polynomial, $n$ is the dimension of the Laplacian stencil, and $\Delta x$ is the spatial discretization size (assuming an equispaced discretization in each direction). This gives us the corresponding band:

$$\Omega_c = \{x : \|\mathbf{x} - CP(\mathbf{x})\|_2 \leq \lambda\}.$$

3. **Embedding**: Next, we embed the surface PDE in $\mathbb{R}^n$ by replacing the surface gradients with the typical gradients in $\mathbb{R}^n$.

4. **Extension**: Finally, extend the initial data from the surface onto the nodes in the computational band by means of the closest point function at each point.

After initializing the closest point method, we proceed by alternating the following two steps until the desired final time is reached.

1. **Extension**: Extend the solution off of the surface onto nodes in the computational band. In practice, this is performed dimension-by-dimension via a barycentric interpolation. The degree of the interpolation polynomials determines the size of the computational band, as stated above.

2. **Solution of PDE in Embedding Space**: Compute the solution of the embedding PDE in $\mathbb{R}^n$ using the typical finite difference schemes in the computational band. This is performed for one time step before repeating the extension step.

The steps presented above are the essence of the closest point method. The method is powerful both in the scope of its application and in its ease of implementation.

### 2.2.1 The Explicit Closest Point Method

The Closest Point Method may be implemented numerically by using an explicit or an implicit time-stepping scheme. We will present the explicit Closest Point Method in this section, the details of which may found in [18]. Consider the following general PDE that allows for advection, diffusion, and reaction:

$$\frac{\partial u}{\partial t} = F(x, u, \nabla_g u, \nabla_g^2 u),$$

where $u : M \to \mathbb{R}$. Assuming a forward Euler time discretization, the corresponding surface evolution problem is stated as:

$$u^{n+1} = u^n + \Delta t \cdot F(x, u, \nabla_g u, \nabla_g^2 u).$$

Instead of dealing with the surface equation directly, we evolve the corresponding equation in the embedding space by means of the closest point operator as follows:

$$u^{n+1} = u^n(CP) + \Delta t \cdot F(CP, u^n(CP), \nabla u^n(CP), \nabla^2 u^n(CP)),$$

where $\nabla$ and $\nabla^2$ are the standard derivative operators in $\mathbb{R}^n$ which may be discretized on an equally-spaced regular grid in $\mathbb{R}^n$, and $CP$ is the closest point function at a give point $x \in S$. In practice, we generally use a second-order centred five-point stencil. As an example we will give the discretization of the in-surface heat equation on a surface embedded in $\mathbb{R}^3$:

**Example:** Consider the in-surface heat equation for a surface $S$ embedded in $\mathbb{R}^n$:

$$\frac{\partial u}{\partial t} = \Delta_S u$$
$$u(\theta, \varphi, 0) = \cos(\varphi).$$

Using an explicit-Euler method with a second-order centred in space scheme gives us:

$$u^{n+1}(CP) = u^n(CP) + \Delta t \cdot \left( \frac{u^n_{i+1,j,k}(CP) + u^n_{i,j+1,k}(CP) + u^n_{i,j,k+1}(CP) - 4u^n_{i,j,k}(CP) + u^n_{i-1,j,k}(CP) + u^n_{i,j-1,k}(CP) + u^n_{i,j,k-1}(CP)}{(\Delta x)^3} \right) \tag{2.1}$$

In practice it is generally more efficient to use an implicit method for discretizing and numerically solving the heat equation. The details on how to perform an implicit solution of in-surface heat flow with the closest point method can be found in [13]. Throughout this thesis we will use the explicit Closest Point Method since it is generally more straightforward to implement.

In the present example, we can either compare the computed solution to the corresponding spherical harmonic expansion, or to the exact solution given by:

$$u_S(\theta, \varphi, t) = e^{-2t} \cos(\varphi).$$

After applying the Closest Point Method with the stencil given in equation (2.1) to this problem, we obtain the following convergence study with discretizations $h = [1/10, 1/20, 1/40, 1/80]$.

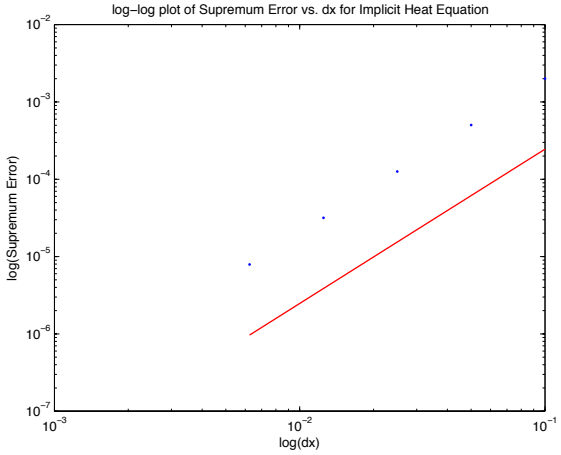


In the figure above, the slope of the line that the data point lie along is $m \approx 1.96$. This demonstrates second order convergence of the closest point method for this particular test-case.

# Chapter 3

# Further Geometric Techniques

In this chapter, we present two geometric techniques. The first is a method from algebraic geometry that is used to resolve singularities. The technique revolves around the 'blow-up' of a singularity which transforms a singular manifold and produces an analogous one that no longer has a geometric singularities. The second technique is an idea from Riemannian geometry that transforms the Laplace-Beltrami operator in such a way that a PDE may be evolved on a given manifold $\tilde{M}$ that actually corresponds to an evolution on a related manifold $M$. These two geometric techniques will be of vital importance to us as we construct a numerical method for evolving PDEs on domains with singularities.

## 3.1 Algebraic Resolution of Singularities

We now turn our attention to the resolution of domains that contain singularities. Clearly, this is an important as a given domain that contains a singularity fails to be Riemannian, and therefore the Laplace-Beltrami operator cannot be posed on the domain in the classical sense.

We will define a singularity in terms of the Jacobian of the given coordinate system. In particular, a singularity arises at a point $p \in M$ when $\det(J(p)) = 0$. Since the metric tensor can be expressed as $g_{ij} = J^T J$, it will also hold that $\det(g^{ij}(p)) = 0$, demonstrating that the manifold fails to be Riemannian at the given point. Moreover, at the point $p \in M$, by the inverse function theorem, we are unable to locally invert the mapping from $\mathbb{R}^n$ to the manifold $M$ that is encoded by the given Jacobian $J$. Consequently, the closest point

method will fail to work at singular points on $M$. In the discussion that follows, we will present a technique for resolving singularities which is somewhat ubiquitous in the field of algebraic geometry.

### 3.1.1 Resolution of Singularities via Blow-Up

We will now present the idea of a blow-up which is a birational transformation that replaces a singular point (or set of points) with the projectivized tangent space at the given point. For our purposes, it will suffice to construct the blow-up extrinsically since we will generally be concerned with how the blown-up manifold is embedded in the ambient (Euclidean) space. Let's proceed with an example to clarify the blow-up transformation.

We will work through the blow-up of the cuspidal curve $y^2 = x^3$ which has a singularity at in the derivative at the origin $(0, 0)$ in $\mathbb{R}^2$. We start by introducing an homogeneous coordinate system for affine space and the projective line:

$$\mathbb{A}^2 \leftrightarrow (x_0, x_1)$$
$$\mathbb{P}^1 \leftrightarrow (y_0, y_1).$$

In this coordinate system, our original curve is given by $x_1^2 = x_0^3$. In order to find point(s) at which this curve may have singularities, we express it in the form of an algebraic variety:

$$w : p(x_0, x_1) = x_1^2 - x_0^3 = 0.$$

To find the singularity, we look at the Jacobian:

$$\begin{cases} \partial p/\partial x_0 &= -3x_0^2 \\ \partial p/\partial x_1 &= 2x_1 \end{cases}$$

The blow-up is subject to the constraint:

$$\left\{ ((x_0, x_1), [y_1 : y_0]) \,\middle|\, \det \begin{vmatrix} x_0 & x_1 \\ y_0 & y_1 \end{vmatrix} = 0 \right\}$$

Now, using the blow-up condition, we have:

$$\begin{vmatrix} x_0 & x_1 \\ y_0 & y_1 \end{vmatrix} = 0$$

which implies

$$y_0 p_1 - y_1 p_0 = 0.$$

Now, we may re-write $w$ in terms of $p_0$ and $p_1$ using the blow-up condition $p_1 = p_0 y_1 / y_0$ for $y_0 \neq 0$, so that:

$$\begin{aligned} p_1^2 - p_0^3 &= \left(\frac{p_0 y_1}{y_0}\right)^2 - p_0^3 \\ &= p_0^2 y_1^2 - p_0^3 y_0^2. \end{aligned}$$

Now consider the chart $y_1 = 1 \Rightarrow p_1 y_0 = p_0$ together with $p_1^2 - p_0^3 = 0$ characterize the blow-up $w$. Now we proceed by substituting as follows:

$$\begin{aligned} p_1^2 - p_0^3 &= 0 \\ p_1^2 - (p_1 y_0)^3 &= 0 \\ p_1^2 (1 - p_1 y_0^3) &= 0. \end{aligned}$$

Now consider the chart $y_0 = 1 \Rightarrow p_1 = p_0 y_1$ together with $p_1^2 - p_0^3 = 0$ characterize $w$. Proceed as follows:

$$\begin{aligned} p_1^2 - p_0^3 &= 0 \\ (p_0 y_1)^2 - p_0^3 &= 0 \\ p_0^2 (y_1^2 - p_0) &= 0. \end{aligned}$$

Now, the blow-up takes the form:

$$\begin{aligned} q_0(x_0, x_1, y_1) &= p_1 - p_0 y_1 \\ &= x_1 - x_0 y_1 \end{aligned}$$

and

$$\begin{aligned} q_1(x_0, x_1, y_1) &= y_1^2 - p_0 \\ &= y_1^2 - x_0. \end{aligned}$$

From the expression for $q_0(x_0, x_1, y_1)$, we get $x_0 = x_1 / y_1$, and from the second expression, we get $x_0 = y_1^2$. This leads to the following parametrization of the blown-up space:

$$\begin{cases} x_0 \mapsto t^2 \\ x_1 \mapsto t^3 \\ y_1 \mapsto t \end{cases} \Rightarrow \begin{cases} x \mapsto t^2 \\ y \mapsto t^3 \\ z \mapsto t \end{cases}$$

Below is a plot of the base curve along with its blow up.

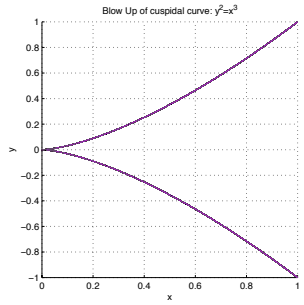


(a) View of the $xy$-plane

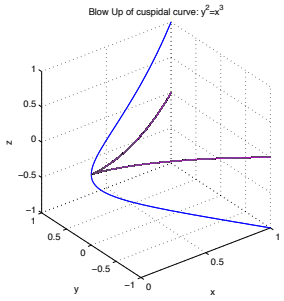


(b) Rotation in $\mathbb{R}^3$

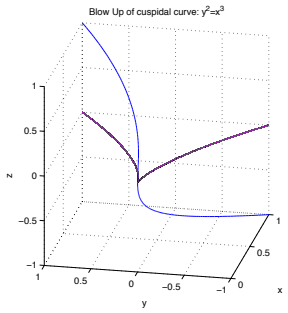


(c) A second rotation in $\mathbb{R}^3$

Figure 3.1: Above are three different views of the curve $\mathcal{C}(t) = (t^2, t^3)$ along with its blow up $\mathcal{C}(t) = (t^2, t^3, t)$. Figure (a) is a view of the $xy$-plane from above, and (b) and (c) are two rotations in $\mathbb{R}^3$.

### 3.1.2 Generalization of Blow-Up Transformation

In the section above, we computed the blow-up for a special case that we represented as an algebraic variety in affine space. More generally, we can view a blow-up as an operation that causes the following diagram to commute:

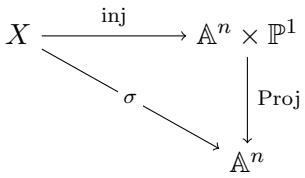


We may generalize the blow-up operation by giving an intrinsic construction. This is done by using coordinate on the normal space to the given point in question. In this case, $N = (x, y)$

becomes the maximal ideal at the origin and $N/N^2$ becomes the normal space at the origin. In this case, the projectivization of the normal space becomes:

$$X = \text{Proj} \bigoplus_{j=0}^{\infty} \text{Sym}^j_{k[x_i,y_i]} N/N^2.$$

In our case above, this expression reduces down to:

$$X = \text{Proj } k[x_0, x_1, y_0, y_1]/(x_0y_1 - x_0y_0).$$

A more thorough and detailed explanation of this is given in [7] by Hartshorne. Below is a pictorial representation of the blow-up of the curve discussed above that represents the geometric view of the blow-up given in this section.

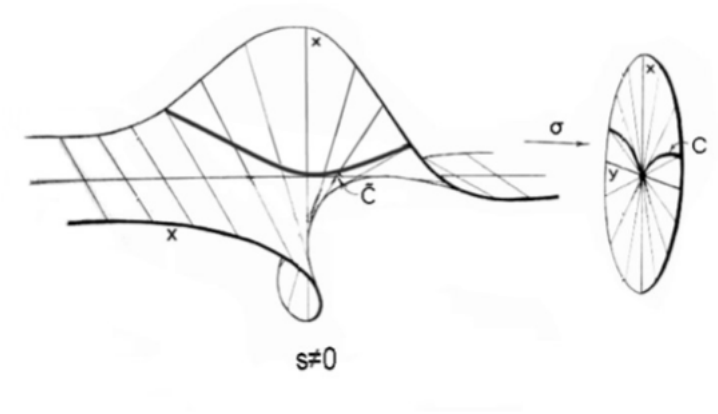


Figure 3.2: Above is a pictorial representation of the blow-up of the cuspidal curve $y^2 = x^3$.

We will finish this chapter by presenting a trick from Riemannian geometry that will allow us to carry out calculations with PDEs that are posed on blown-up domains.

## 3.2 A Differential-Geometric Trick

Recall that the Laplace-Beltrami operator may be expressed as follows:

$$\Delta_g u = -\frac{1}{\sqrt{|g|}} \frac{\partial}{\partial x^j} \left( \sqrt{|g|} g^{ij} \frac{\partial u}{\partial x^i} \right).$$

One can check that if the metric tensor $g_{ij}$ is set to be the typical Euclidean metric $g_{ij} = (\delta_{ij})$, then the above expression reduces to the classical Laplacian. It is clear that this is a special case since for this choice of $g_{ij}$ the components of the metric tensor do not depend on coordinate system $(x^1, \ldots, x^n)$, thereby eliminating any differential cross terms in the final expression of the Laplacian. In general, however, the metric tensor $g_{ij}$ will depend on the coordinates $(x^1, \ldots, x^n)$, and therefore the Laplace-Beltrami operator may have several differential cross-terms. For example, in the expression for the spherical

$$\Delta u = \frac{1}{r^2}\frac{\partial}{\partial r}\left(r^2\frac{\partial u}{\partial r}\right) + \frac{1}{r^2\sin\theta}\frac{\partial}{\partial\theta}\left(\sin\theta\frac{\partial u}{\partial\theta}\right) + \frac{1}{r^2\sin^2\theta}\frac{\partial^2 u}{\partial\varphi^2}.$$

In this case, the non-trivial dependence of the differential terms involving $r$ and $\varphi$ encode the geometry of the underlying manifold into the spherical Laplacian. Furthermore, it is crucial to note that in general the Laplace-Beltrami operator incorporates information regarding the structure of the underlying manifold itself.

Often times, however, we may want to evolve a differential operator on one manifold that corresponds to a differential equation posed on another. In the following subsection, we present an example that demonstrates precisely this idea.

### 3.2.1 Example: Function over a Circle

Let us consider a circle in $\mathbb{R}^2$ which we may parametrize as $(r\cos\theta, r\sin\theta)$. Using the coordinate definition of the Laplace-Beltrami operator, we may calculate the Laplacian in polar coordinates as:

$$\begin{aligned}\Delta u &= \frac{1}{r}\frac{\partial}{\partial r}\left(r\frac{\partial u}{\partial r}\right) + \frac{1}{r^2}\frac{\partial^2 u}{\partial\theta^2} \\ &= \frac{1}{r}\frac{\partial u}{\partial r} + \frac{\partial^2 u}{\partial r^2} + \frac{1}{r^2}\frac{\partial^2 u}{\partial\theta^2}.\end{aligned}$$

Now, we will restrict our attention to the unit circle, in which case our parametrization is given by $(\cos\theta, \sin\theta)$ and the corresponding Laplace operator simplifies to

$$\Delta u = \frac{\partial^2 u}{\partial\theta^2}.$$

Now, suppose we consider a function, say $h(\theta)$ that acts over the circle so that its parametrization is given by $(\cos\theta, \sin\theta, h(\theta))$. The corresponding metric tensor has only one component

and is given by:

$$\begin{aligned} g_{ij} &= \frac{\partial u}{\partial x^i} \cdot \frac{\partial u}{\partial x^j} \\ &= \sin^2\theta + \cos^2\theta + [h'(\theta)]^2 \\ &= 1 + [h'(\theta)]^2. \end{aligned}$$

The corresponding Laplace-Beltrami operator is given by:

$$\begin{aligned} \Delta_g u &= \frac{1}{\sqrt{1+[h'(\theta)]^2}} \frac{\partial}{\partial\theta} \left( \sqrt{1+[h'(\theta)]^2} \frac{1}{1+[h'(\theta)]^2} \frac{\partial u}{\partial\theta} \right) \\ &= \frac{1}{\sqrt{1+[h'(\theta)]^2}} \frac{\partial}{\partial\theta} \left( \frac{1}{\sqrt{1+[h'(\theta)]^2}} \frac{\partial u}{\partial\theta} \right). \end{aligned}$$

Now, the reader will notice that the above expression differs from the Laplacian on the unit circle by a factor of $1/\sqrt{1+[h'(\theta)]^2}$. Moreover, we may transform the expression for the Laplacian on the domain defined by a function over the unit circle to the Laplacian over the unit circle by means of a variable coefficient $\kappa$:

$$\Delta_{\mathbb{S}^2} u = \frac{\kappa}{\sqrt{1+[h'(\theta)]^2}} \frac{\partial}{\partial\theta} \left( \frac{\kappa}{\sqrt{1+[h'(\theta)]^2}} \frac{\partial u}{\partial\theta} \right).$$

where $\kappa := \sqrt{1+[h'(\theta)]^2}$. This will prove useful in later sections when we deal with implementing the closest point method on domains that are 'blown-up'. We will now proceed to generalize the above idea.

### 3.2.2 Generalization of the Differential-Geometric trick

The technique introduced in the previous section may be generalized to a deeper geometric idea by dealing the with the underlying metric tensors of the given manifolds directly. We will briefly present an argument that extends the principle. In the discussion that follows, we will let $(M, g_{ij})$ be our base manifold and we will let $(\tilde{M}, \tilde{g})$ denote the manifold which is a transformed version of the original manifold. now, clearly, the Laplace-Beltrami operator over the manifold $(\tilde{M}, \tilde{g})$ is given by:

$$\Delta_{\tilde{g}} u = -\frac{1}{\sqrt{|\tilde{g}|}} \frac{\partial}{\partial x^j} \left( \sqrt{|\tilde{g}|} \tilde{g}^{ij} \frac{\partial u}{\partial x^i} \right).$$

Now, our goal is to transform the above Laplacian to one that operates over the original Laplacian $\Delta_g u$. Observe that we may transform in the following manner:

$$\begin{aligned}\Delta_g u &= -\frac{1}{\sqrt{|\tilde{g}|}}\left[\frac{\sqrt{|\tilde{g}|}}{\sqrt{|g|}}\right]\frac{\partial}{\partial x^j}\left(\sqrt{|\tilde{g}|}\tilde{g}^{ij}\left[\frac{\sqrt{|g|}}{\sqrt{|\tilde{g}|}}\tilde{g}_{ij}g^{ij}\right]\frac{\partial u}{\partial x^i}\right)\\ &= \frac{1}{\sqrt{|g|}}\frac{\partial}{\partial x^j}\left(\sqrt{|g|}g^{ij}\frac{\partial u}{\partial x^i}\right),\end{aligned}$$

where the final step is obtained through cancelation properties of the metric tensors. For a one-dimensional manifold such as the one presented in the previous section this process can be thought of geometrically as scaling the differential operator by a magnitude that is proportional to the projection of the tangent vector at a given point onto the $xy$-plane. Hence, intuitively, the variable coefficient causes 'heat' to 'flow' faster on portions of the curve that deviate more significantly from the base manifold.

The strength of this technique is derived from the fact that we can alter the differential structures posed on a given domain to coincide with, and hence solve, a PDE that is posed a similar underlying manifold. We will use this fact in the sections that follow to map differential structures through a blow-up chart on a singular manifold. Ultimately, this will allow us to solve a heat equation on a blown-up domain that corresponds to a heat equation on the original domain.

# Chapter 4

# Solution of the Heat Equation on Singular Domains

At this point, we have the main components necessary to construct a method for evolving the heat equation on a manifold with a singularity. We will focus our attention on the example $y^2 = x^3$ as this is a natural problem to test our methods on, and the techniques that we use on this problem should generalize to higher dimensional manifolds with similar singularities.

## 4.1 Constructing a Closure of the Domain

In order to make the calculation more manageable, we will construct a closure for the set $X(t) := \{(x, y, z) : (t^2, t^3, t)\}$. This will be done by truncating the curve $X(t)$ at a fixed point and constructing a parametrized curve in $\mathbb{R}^3$ that connects the end points and satisfies the condition that new domain is everywhere $C^2$.

More explicitly, we truncate the curve $X(t)$ by making the restriction $t \in [-1, 1]$, call this truncation $\tilde{X}(t)$. To this curve, we adjoin another curve $\mathcal{C}(t)$ with the following properties: $\mathcal{C}(-1) = \tilde{X}(-1)$, $\mathcal{C}'(-1) = \tilde{X}'(-1)$, and $\mathcal{C}''(-1) = \tilde{X}''(-1)$ and also $\mathcal{C}(1) = \tilde{X}(1)$, $\mathcal{C}'(1) = \tilde{X}'(1)$, and $\mathcal{C}''(1) = \tilde{X}''(1)$. This uniquely determines a fifth degree polynomial in $t$ for each

of the components $(x, y, z)$. This polynomial can be written down explicitly as:

$$\mathcal{C}(t) = \begin{pmatrix} t^5 + 9\,t^4 + 31\,t^3 + 50\,t^2 + 36\,t + 10 \\ -15\,t^5 - 116\,t^4 - 347\,t^3 - 498\,t^2 - 341\,t - 90 \\ -6\,t^5 - 46\,t^4 - 136\,t^3 - 192\,t^2 - 129\,t - 34 \end{pmatrix} \tag{4.1}$$

for $t \in [-1, -2]$ and

$$\mathcal{C}(t) = \begin{pmatrix} -t^5 + 9\,t^4 - 31\,t^3 + 50\,t^2 - 36\,t + 10 \\ -15\,t^5 + 116\,t^4 - 347\,t^3 + 498\,t^2 - 341\,t + 90 \\ -6\,t^5 + 46\,t^4 - 136\,t^3 + 192\,t^2 - 129\,t + 34 \end{pmatrix} \tag{4.2}$$

for $t \in [1, 2]$, and it is easy to check that at least two derivatives of $\mathcal{C}(-2)$ agree with the corresponding derivatives for $\mathcal{C}(2)$. Hence, the new curve $\tilde{\mathcal{C}}(t) := \tilde{X}(t) \bigcup \mathcal{C}(t)$ for $t \in [-2, 2]$ is closed and everywhere $C^2$. Henceforth, we will use the curve $\tilde{\mathcal{C}}(t)$ as our blown-up domain.

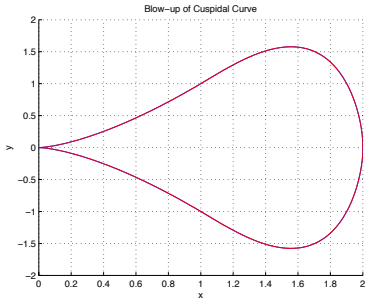


(a) View of the $xy$-plane

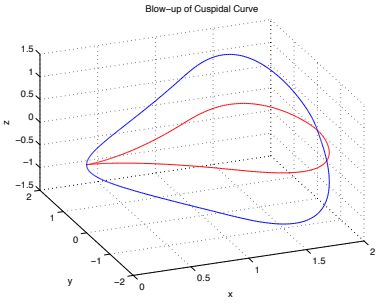


(b) Rotation in $\mathbb{R}^3$

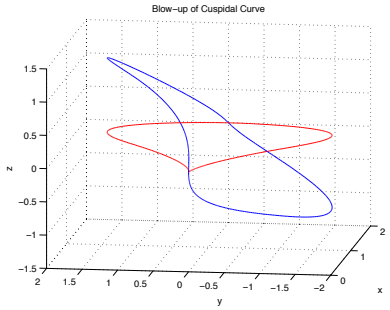


(c) A second rotation in $\mathbb{R}^3$

Figure 4.1: Above are three different views of the space $\tilde{\mathcal{C}}(t) = \tilde{X}(t) \bigcup \mathcal{C}(t)$. Figure (a) is a view of the $xy$-plane from above, and (b) and (c) are two rotations in $\mathbb{R}^3$.

### 4.1.1 Construction of Geometric-Differential Operators for Blown-up and Blown-down Domains

Now that we have constructed our two domains of interest, we will proceed by computing the corresponding metric tensors. Let's start with the blown-down curve which we will denote by $\tilde{\mathfrak{c}}(t)$. The curve $\tilde{\mathfrak{c}}(t)$ is simply the projection of the blown-up curve $\tilde{\mathcal{C}}(t)$ onto the first two coordinates. For simplicity and to avoid unneeded clutter, we will restrict our attention to the component of the curve that contains the cusp, i.e. $t \in [-1, 1]$. The metric for this segment of $\tilde{\mathfrak{c}}(t)$ is computed as follows:

$$\begin{aligned} g_{ij} &= \frac{\partial u}{\partial x^i} \cdot \frac{\partial u}{\partial x^j} \\ &= \langle 2t, 3t^2 \rangle \cdot \langle 2t, 3t^2 \rangle \\ &= 4t^2 + 9t^4. \end{aligned}$$

Immediately, we see that the metric $g_{ij}$ has a singularity when $t = 0$. This is not surprising though, because this is the whole reason that we performed the blow-up operation. We proceed by computing the metric tensor for the blown-up space $\tilde{\mathcal{C}}(t)$.

$$\begin{aligned} \tilde{g}_{ij} &= \frac{\partial u}{\partial x^i} \cdot \frac{\partial u}{\partial x^j} \\ &= \langle 2t, 3t^2, 1 \rangle \cdot \langle 2t, 3t^2, 1 \rangle \\ &= 4t^2 + 9t^4 + 1. \end{aligned}$$

As is evident, the addition of the third component regularizes the metric tensor since now $|\tilde{g}_{ij}| \geq 1$ for all values of $t$. In particular $|\tilde{g}_{ij}| \neq 0$ for any value of $t$, and hence is well-defined and locally invertible at every point in the domain.

These calculations provide some insight into the nature of the corresponding Laplace-Beltrami operators. Let's start by computing the Laplacian for the blown-down curve $\tilde{\mathfrak{c}}(t)$:

$$\begin{aligned} \Delta_g u &= -\frac{1}{\sqrt{|g|}} \frac{\partial}{\partial x^j} \left( \sqrt{|g|} g^{ij} \frac{\partial u}{\partial x^i} \right) \\ &= -\frac{1}{\sqrt{4t^2 + 9t^4}} \frac{\partial}{\partial x^j} \left( \sqrt{4t^2 + 9t^4} \frac{1}{4t^2 + 9t^4} \frac{\partial u}{\partial x^i} \right) \\ &= -\frac{1}{\sqrt{4t^2 + 9t^4}} \frac{\partial}{\partial x^j} \left( \frac{1}{\sqrt{4t^2 + 9t^4}} \frac{\partial u}{\partial x^i} \right). \end{aligned}$$

At this point, we note that the differential operator clearly blows up at $t = 0$ for the curve $\tilde{\mathfrak{c}}(t)$. Now, we compute the Laplace-Beltrami operator for $\tilde{\mathcal{C}}(t)$:

$$\begin{aligned}\Delta_{\tilde{g}} u &= -\frac{1}{\sqrt{|\tilde{g}|}} \frac{\partial}{\partial x^j} \left( \sqrt{|\tilde{g}|} \tilde{g}^{ij} \frac{\partial u}{\partial x^i} \right) \\ &= -\frac{1}{\sqrt{4t^2 + 9t^4 + 1}} \frac{\partial}{\partial x^j} \left( \sqrt{4t^2 + 9t^4 + 1} \frac{1}{4t^2 + 9t^4 + 1} \frac{\partial u}{\partial x^i} \right) \\ &= -\frac{1}{\sqrt{4t^2 + 9t^4 + 1}} \frac{\partial}{\partial x^j} \left( \frac{1}{\sqrt{4t^2 + 9t^4 + 1}} \frac{\partial u}{\partial x^i} \right).\end{aligned}$$

Now, clearly $\Delta_{\tilde{g}}(\cdot)$ is a smooth operator since $\tilde{g}$ is sufficiently regularized.

Recall that we are actually interested in how heat flows on the blown-down curve $\tilde{\mathfrak{c}}(t)$. This is where the differential-geometric trick comes in. We know how to flow heat along the blown-up curve using the closest point method, so now we will evolve a modified equation on the curve $\tilde{\mathcal{C}}(t)$ that coincides with the heat equation on $\tilde{\mathfrak{c}}(t)$. Such an equation is given by:

$$\Delta_g u = \frac{\kappa}{\sqrt{4t^2 + 9t^4 + 1}} \frac{\partial}{\partial x^j} \left( \frac{\kappa}{\sqrt{4t^2 + 9t^4 + 1}} \frac{\partial}{\partial x^i} \right).$$

where

$$\kappa := \frac{\sqrt{4t^2 + 9t^4 + 1}}{\sqrt{4t^2 + 9t^4}}.$$

The benefit of this approach is that the expression for $\Delta_g u$ can be evolved on $\tilde{\mathcal{C}}(t) \subset \mathbb{R}^3$ using the closest point method.

### 4.1.2 Numerical Method

For our purposes, we are interested in constructing a method for evolving the heat equation on a singular domain. Hence, we will use the techniques mentioned above to de-singularize a given domain and subsequently evolve a heat equation on it. To this end, we are interested in solving a heat equation that takes the form

$$u_t = -\frac{1}{\sqrt{|g|}} \frac{\partial}{\partial x^j} \left( \sqrt{|g|} g^{ij} \frac{\partial u}{\partial x^i} \right), \tag{4.3}$$

where the manifold, and hence metric tensor $g$, may have a singularity. This will ultimately produce a variable-coefficient heat equation of the form

$$u_t = -\frac{1}{\sqrt{|\tilde{g}|}} \left[ \frac{\sqrt{|\tilde{g}|}}{\sqrt{|g|}} \right] \frac{\partial}{\partial x^j} \left( \sqrt{|\tilde{g}|} \tilde{g}^{ij} \left[ \frac{\sqrt{|g|}}{\sqrt{|\tilde{g}|}} \tilde{g}_{ij} g^{ij} \right] \frac{\partial u}{\partial x^i} \right). \tag{4.4}$$

We will focus our attention on solving the heat equation posed on the domain that was constructed in the previous section. That is, we will solve the variable-coefficient heat equation given by:

$$u_t = \frac{\kappa}{\sqrt{4t^2+9t^4+1}}\frac{\partial}{\partial x^j}\left(\frac{\kappa}{\sqrt{4t^2+9t^4+1}}\frac{\partial}{\partial x^i}\right).$$

where

$$\kappa := \frac{\sqrt{4t^2+9t^4+1}}{\sqrt{4t^2+9t^4}}.$$

In order to construct a method for this particular PDE, we will begin by solving a typical variable-coefficient heat equation that is defined in typical Euclidean space.

### 4.1.3 Numerical Solution of Variable-Coefficient Heat Equations

We will start by constructing a numerical method for solving the canonical variable-coefficient heat equation in $\mathbb{R}^n$ given by:

$$u_t = \nabla \cdot (\beta(\mathbf{x})\nabla u(\mathbf{x})).$$

Restricting to the $1D$ case, we may approximate the Laplacian term by:

$$\nabla \cdot (\beta(\mathbf{x})\nabla u(\mathbf{x})) \approx \frac{\beta_{i+1/2}\left(\frac{u_{i+1}-u_i}{\Delta x}\right) - \beta_{i-1/2}\left(\frac{u_i-u_{i-1}}{\Delta x}\right)}{\Delta x},$$

where

$$\beta_{i+1/2} = \frac{\beta_i + \beta_{i+1}}{2}.$$

Now, we may use a number of different methods for discretizing the time-component of the PDE. As a starting point, we will use a forward-Euler discretization. Doing so yields the following numerical scheme for the 1D variable-coefficient heat equation:

$$\frac{u_i^{n+1}-u_i^n}{\Delta t} = \frac{\beta_{i+1/2}\left(\frac{u_{i+1}^n-u_i^n}{\Delta x}\right) - \beta_{i-1/2}\left(\frac{u_i^n-u_{i-1}^n}{\Delta x}\right)}{\Delta x}$$

In 2D the corresponding numerical scheme becomes:

$$\frac{u_{i,j}^{n+1}-u_{i,j}^n}{\Delta t} = \frac{\beta_{i+1/2}\left(\frac{u_{i+1,j}^n-u_{i,j}^n}{\Delta x}\right) - \beta_{i-1/2}\left(\frac{u_{i,j}^n-u_{i-1,j}^n}{\Delta x}\right)}{\Delta x} + \frac{\beta_{j+1/2}\left(\frac{u_{i,j+1}^n-u_{i,j}^n}{\Delta y}\right) - \beta_{j-1/2}\left(\frac{u_{i,j}^n-u_{i,j-1}^n}{\Delta y}\right)}{\Delta y}.$$

It is easy to see that this discretization of the Laplacian generalizes to $\mathbb{R}^N$ via the following expression:

$$\frac{u_i^{n+1}-u_i^n}{\Delta t} = \sum_{i=1}^{N} \frac{\beta_{i+1/2}\left(\frac{u_{i+1}^n-u_i^n}{\Delta x^i}\right) - \beta_{i-1/2}\left(\frac{u_i^n-u_{i-1}^n}{\Delta x^i}\right)}{\Delta x^i}, \tag{4.5}$$

where $x^i$ represents the $i$th coordinate in $\mathbb{R}^N$. This gives us a forward-Euler discretization for the variable coefficient heat equation in $\mathbb{R}^n$.

### 4.1.4 Solution of Variable-Coefficient Geometric PDEs via the Closest Point Method

At this point we have all of the required tools to construct a method for solving geometric PDEs of the form (4.4). We will do this by computing the closest points on the domain corresponding to (4.3) then we will evolve the corresponding heat equation as a variable-coefficient PDE where the coefficients correspond to the additional terms added in (4.4). In effect, we are evolving a heat equation so that the rate of diffusion corresponds to the lengthening of the blown-up curve $\tilde{\mathcal{C}}(t)$ with respect to the original curve $\tilde{\mathfrak{c}}(t)$.

Recall, the closest point method can be used to compute solutions to problems of the form (4.3). By making the identifications

$$\nabla u(CP) = \nabla_s u$$

and

$$\nabla \cdot v(CP) = \nabla_s \cdot v,$$

we can write the surface Laplacian as:

$$\nabla \cdot (\nabla u(CP)) = \nabla_s \cdot (\nabla_s u).$$

Therefore, in the in-surface heat equation

$$\begin{aligned} u_t &= \Delta_s u, \\ u(0, \mathbf{x}) &= u_0(\mathbf{x}) \end{aligned}$$

we may replace the Laplace-Beltrami operator with the standard Laplacian by replacing the spacial components on the right-hand-side with the closest point function. This yields the embedding PDE given by:

$$\begin{aligned} u_t(t, \mathbf{x}) &= \Delta(u(t, cp(\mathbf{x}))), \\ u(0, \mathbf{x}) &= u_0(cp(\mathbf{x})), \end{aligned}$$

which agrees with the in-surface heat flow on the surface itself. By applying the closest point method, we can numerically solve the in-surface heat flow PDE given above. However, we

actually want to solve a PDE of the form (4.4). As we noted above, we can view equation (4.4) as a variable coefficient heat equation with respect to (4.3). Hence, we will proceed by computing the closest point representation of the curve or surface $\tilde{\mathcal{C}}(t)$ which corresponds to (4.3) and then we will use this representation to evolve a variable-coefficient heat equation of the form (4.4) which will give us the evolution of the typical constant-coefficient heat equation on $\tilde{\mathfrak{c}}(t)$. In particular, our variable-coefficient takes the form:

$$\beta(\mathbf{x}) = \frac{\sqrt{|g|}}{\sqrt{\tilde{g}}}\tilde{g}_{ij}g^{ij}(\mathbf{x}).$$

In terms of the closest point representation we have:

$$\beta(CP(\mathbf{x})) = \frac{\sqrt{|g|}}{\sqrt{\tilde{g}}}\tilde{g}_{ij}g^{ij}(CP(\mathbf{x})).$$

Now, we may apply the discretization given in (4.5), where the variable-coefficient is the choice of $\beta(\mathbf{x})$ or $\beta(CP(\mathbf{x}))$ given above, corresponding to the in-surface flow versus the closest point representation. If we want to evolve a variable-coefficient heat equation of this nature on a curve in $\mathbb{R}^3$, then equation (4.5) will take the form:

$$\frac{u_i^{n+1}(\mathbf{x}) - u_i^n(CP(\mathbf{x}))}{\Delta t} =$$
$$\alpha(CP(\mathbf{x}))\sum_{i=1}^{3}\frac{\beta_{i+1/2}(CP(\mathbf{x}))\left(\frac{u_{i+1}^n(CP(\mathbf{x}))-u_i^n(CP(\mathbf{x}))}{\Delta x^i}\right) - \beta_{i-1/2}(CP(\mathbf{x}))\left(\frac{u_i^n(CP(\mathbf{x}))-u_{i-1}^n(CP(\mathbf{x}))}{\Delta x^i}\right)}{\Delta x^i},$$

where

$$\alpha(CP(\mathbf{x})) = \frac{\sqrt{|\tilde{g}|}}{\sqrt{|\tilde{g}|}}(CP(\mathbf{x})).$$

This gives us a discretization of

$$u_t = -\frac{1}{\sqrt{|\tilde{g}|}}\left[\frac{\sqrt{|\tilde{g}|}}{\sqrt{|g|}}\right]\frac{\partial}{\partial x^j}\left(\sqrt{|\tilde{g}|}\tilde{g}^{ij}\left[\frac{\sqrt{|g|}}{\sqrt{|\tilde{g}|}}\tilde{g}_{ij}g^{ij}\right]\frac{\partial u}{\partial x^i}\right)$$

by means of the closest point representation.

## 4.2 A Further Investigation of Computing on Singular Domains

Recall that in this chapter we are particularly concerned with the cuspidal domain generated by the curve $y^2 = x^3$ and its corresponding blow up. The corresponding heat equation on

the singular domain is given by

$$u_t = \frac{1}{\sqrt{4t^2+9t^4}} \frac{\partial}{\partial x^j} \left( \frac{1}{\sqrt{4t^2+9t^4}} \frac{\partial u}{\partial x^i} \right).$$

The corresponding variable-coefficient heat equation on the blown-up domain is given by:

$$u_t = \frac{\kappa}{\sqrt{4t^2+9t^4+1}} \frac{\partial}{\partial x^j} \left( \frac{\kappa}{\sqrt{4t^2+9t^4+1}} \frac{\partial}{\partial x^i} \right).$$

where

$$\kappa := \frac{\sqrt{4t^2+9t^4+1}}{\sqrt{4t^2+9t^4}}.$$

Now, we will note that $\kappa(t)$ has a singularity at $t = 0$. This corresponds to the cusp that appears at that point in the domain $\tilde{\mathfrak{c}}(t)$. Physically, this tells us that heat has to flow infinitely quickly past the point $t = 0$ in the blown-up domain in order to correspond with heat flow in the blown-down domain. In practice, we smooth out this singularity by adding an $\varepsilon$ term as follows:

$$\kappa \approx \frac{\sqrt{4t^2+9t^4+1}}{\sqrt{4t^2+9t^4+\varepsilon}}.$$

In order to be safe, we generally take $\varepsilon \leq (\Delta x)^4$. This guarantees that the smoothing of $\kappa(t)$ is well below the grid resolution size, yet at the same time it is not so large as to distort our other calculations.

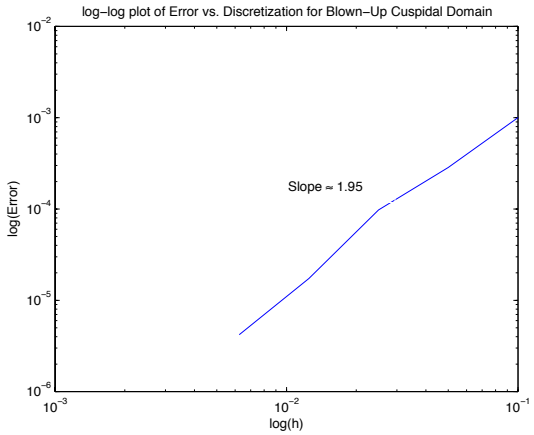


In the plot above, we plot the error in the variable-coefficient heat equation scheme for evolving a PDE on our blown-up domain $\tilde{\mathcal{C}}(t)$ that corresponds to heat on the blown-down domain $\tilde{\mathfrak{c}}(t)$. The discretization sizes used were $h = [.1, .05, .025]$. For this case, we used an explicit scheme in order to avoid the severe stability condition introduced by terms around

the singularity. Hence, we used a time step of $dt = .0001$. We evolved the solution to a final time of $t_{\text{final}} = .025$, in order to investigate the short-time convergence of the solution. The solution was compared with the evolution of a heat equation on a segment in $\mathbb{R}^1$ with the same arclength and periodic boundary conditions. In the plot above, the slope of the line is $m \approx 1.95$, which suggests second order convergence for short-time evolutions.

# Chapter 5

# Future Work and Directions

In this thesis we presented several new techniques that ultimately culminated in a novel approach to evolving time-dependent PDEs on domains with geometric singularities. Many of the techniques that were developed in this direction are of interest and have further applications in their own right. As a conclusion to this work, we discuss several possible extensions, many of which are quite tractable.

- Perhaps one of the first steps is to analytically prove that the numerical method presented in this thesis converges to the Friedrichs solution for general manifolds with singularities. A significant step in this direction would be to demonstrate that by solving the variable-coefficient equation with smooth differential coefficients, we are in fact performing a mollification of the given singular domain. This would then demonstrate that the evolution of the heat equation with the Laplace-Beltrami operator on the corresponding sequence of mollified domains converges to the Friedrichs solution for the given problem.
- In this thesis we chose to work with the problem of evolving the heat equation on the singular domain given by $y^2 = x^3$. In this particular case, the underlying manifold is simply a curve, i.e. a 1-dimensional manifold. It is possible that by restricting ourselves to work with a manifold that is only 1-dimensional that much of the deeper topological and geometric ideas involving singularities are overlooked. It is also possible that lower-dimensional cases are in some sense more difficult to deal with. In the future one might envision applying this method to a cone-type singularity in which

the the manifold is of dimension two or higher everywhere except at the point of singularity where it reduces to dimension zero. One of the benefits of considering cone-type singularities is that there is considerable literature on the topic with the initial approach to the problem due to J. Cheeger in [3].

- In order to make the process present fully automated, one might construct a homotopy-based geometric flow that produces the blow-up of the given singularity.

- I would also like to explore the idea of developing a computational approach to spectral geometry. Spectral Geometry studies the spectrum of operators like the canonical parabolic operator (i.e., Laplace-Beltrami). One of the fundamental concepts of spectral geometry is that given a Laplace operator on a compact Riemannian manifold, the spectrum will indicate properties such as the topology of the underlying manifold as well as how the manifold curves through space. There are many interesting questions in spectral geometry that are still open, and the closest point method could be used as an effective tool in obtaining data related to conjectures in the field.

# Appendix A

# Finding Closest Points

In this appendix, we construct a method for finding closest point operators for parametrized curves in $\mathbb{R}^3$. The method performs a Newton's-method (locally) zero-find on a particular minimization problem. We will demonstrate this by working the the parameterization for out blown-up manifold $\tilde{\mathfrak{c}}(t)$:

$$\tilde{\mathfrak{c}}(t) = \begin{pmatrix} t^2 \\ t^3 \\ t \end{pmatrix},$$

which is the blow-up of $y^2 = y^3$ at the origin.

Now we want to compute the Euclidean distance between a point $(x_0, y_0, z_0) \in \mathbb{R}^3$ and the curve at a general point. The formula is given by:

$$d(\mathbf{x}_0, \Gamma(t)) = \sqrt{(x_0 - t)^2 + (y_0 - t^3)^2 + (z_0 - t)^2}.$$

Now, in order to optimize this take it derivative:

$$d'(\mathbf{x}_0, \Gamma(t)) = \frac{2(x_0 - t) \cdot (-2t) + 2(y_0 - t^3) \cdot (-3t^2) + 2(z_0 - t) \cdot (-1)}{\sqrt{(x_0 - t)^2 + (y_0 - t^3)^2 + (z_0 - t)^2}}.$$

Now we want to locally set $d'(\mathbf{x}_0, \Gamma(t)) = 0$ and find the corresponding value of $t$, which will give us the closest point $CP(\mathbf{x}_0) \in \Gamma(t)$. Moreover, given that $\sum_i (x_i - x_i(t))^2 \neq 0$ we can make the following simplification:

$$d'(\mathbf{x}_0, \Gamma(t)) = 0 \Rightarrow 2(x_0 - t) \cdot (-2t) + 2(y_0 - t^3) \cdot (-3t^2) + 2(z_0 - t) \cdot (-1) = 0.$$

At this point, we proceed by finding a zero of $f(t)$ with respect to $t$ by using Newton's method given by:

$$t_{n+1} = t_n - \frac{f(t_n)}{f'(t_n)}.$$

Computing the derivative of $f(t)$ with respect to $t$ gives us:

$$f'(t) = 2(-2t)(-2t) + 2(x_0 - t^2)(-2) + 2(-3t^2)(-3t^2) + 2(y_0 - t^3)(-6t) + 2.$$

Now, we have all of the components needed to perform Newton's method, except for an initial guess.

For the initial guess, in practice, the domain is subdivided into a finite number of intervals (generally around 100-500 subintervals), and we then evaluate $x(t)$ at each of these points. Following this, we then compute the distance between these points and $(x_0, y_0, z_0)$ and then minimize over the distance. This gives a relatively accurate initial guess. Overall, this method is able to produce the closest point operator for a given node in $\mathbb{R}^3$ to machine precision in under a second.

# Appendix B

# Arclength for Blown-Up Cuspidal Curve

As derived earlier in the thesis, the parameterization for the blow-up of $y^2 = x^3$ is:

$$\tilde{\mathfrak{c}}(t) = \begin{pmatrix} t^2 \\ t^3 \\ t \end{pmatrix},$$

with a $C^2$ closure given by:

$$\mathcal{C}(t) = \begin{pmatrix} t^5 + 9\,t^4 + 31\,t^3 + 50\,t^2 + 36\,t + 10 \\ -15\,t^5 - 116\,t^4 - 347\,t^3 - 498\,t^2 - 341\,t - 90 \\ -6\,t^5 - 46\,t^4 - 136\,t^3 - 192\,t^2 - 129\,t - 34 \end{pmatrix}$$

for $t \in [-1, -2]$ and

$$\mathcal{C}(t) = \begin{pmatrix} -t^5 + 9\,t^4 - 31\,t^3 + 50\,t^2 - 36\,t + 10 \\ -15\,t^5 + 116\,t^4 - 347\,t^3 + 498\,t^2 - 341\,t + 90 \\ -6\,t^5 + 46\,t^4 - 136\,t^3 + 192\,t^2 - 129\,t + 34 \end{pmatrix}$$

for $t \in [1, 2]$.

Now, we may compute the arclength of each of the segments $\Gamma_1, \Gamma_2, \Gamma_3$ by means of the arclength formula:

$$S(t) = \sum_i \int_{\Gamma_i} \sqrt{\sum_{i=1}^{n} (x_i'(t))^2} dt.$$

Computing the derivative of each of the components gives us:

$$\tilde{\mathfrak{c}}'(t) = \begin{pmatrix} t^2 \\ t^3 \\ t \end{pmatrix},$$

with a $C^2$ closure given by:

$$\mathcal{C}'(t) = \begin{pmatrix} 5t^4 + 36\,t^3 + 93\,t^2 + 100\,t + 36 \\ -75\,t^4 - 464\,t^3 - 1041\,t^2 - 996\,t - 341 \\ -30\,t^4 - 184\,t^3 - 408\,t^2 - 384\,t - 129 \end{pmatrix}$$

for $t \in [-1, -2]$ and

$$\mathcal{C}'(t) = \begin{pmatrix} -5t^4 + 36\,t^3 - 93\,t^2 + 100\,t - 36 \\ -75\,t^4 + 464\,t^3 - 1041\,t^2 + 996\,t - 996\,t - 341 \\ -30\,t^4 + 184\,t^3 - 408\,t^2 + 384\,t - 129 \end{pmatrix}$$

for $t \in [1, 2]$.

Applying the arclength formula gives us on $\Gamma_1(t)$:

$$\begin{aligned} S_1(t) = \int_{-2}^{-1} [&(5t^4 + 36\,t^3 + 93\,t^2 + 100\,t + 36)^2 \\ &+ (-75\,t^4 - 464\,t^3 - 1041\,t^2 - 996\,t - 341)^2 \\ &+ (-30\,t^4 - 184\,t^3 - 408\,t^2 - 384\,t - 129)^2]^{1/2} dt \\ &\approx 2.88957. \end{aligned}$$

On $\Gamma_2(t)$ the arclength is given by:

$$\begin{aligned} S_2(t) &= \int_{-1}^{1} \sqrt{(2t)^2 + (3t^2)^2 + (1)^2} dt \\ &\approx 3.72605. \end{aligned}$$

Finally, the arclength of $\Gamma_3(t)$ is the same as on $\Gamma_1(t)$:

$$\begin{aligned} S_3(t) = \int_{-2}^{-1} [&(-5t^4 - 36\,t^3 - 93\,t^2 - 100\,t - 36)^2 \\ &+ (-75\,t^4 + 464\,t^3 - 1041\,t^2 + 996\,t - 341)^2 \\ &+ (-30\,t^4 + 184\,t^3 - 408\,t^2 + 384\,t - 129)^2]^{1/2} dt \\ &\approx 2.88957. \end{aligned}$$

The total arclength of the complete curve is given by:

$$S(t) = \sum_i \int_{\Gamma_i} \sqrt{\sum_{i=1}^{n} (x_i'(t))^2} dt \approx 9.50519.$$

# Bibliography


[1] I. Chavel. *Eigenvalues in Riemannian geometry*, volume 115. Academic Pr, 1984.

[2] I. Chavel. *Isoperimetric inequalities: differential geometric and analytic perspectives*. Number 145. Cambridge Univ Pr, 2001.

[3] J. Cheeger. Spectral geometry of singular riemannian spaces. *J. Differential Geom*, 18(4):575–657, 1983.

[4] M.P. Do Carmo. *Riemannian geometry*. Birkhauser, 1992.

[5] P. Griffiths and J. Harris. *Principles of algebraic geometry*, volume 52. Wiley-interscience, 2011.

[6] J. Harris. *Algebraic geometry: a first course*, volume 133. Springer, 1992.

[7] R. Hartshorne. *Algebraic geometry*, volume 52. Springer, 1977.

[8] J. Jost. *Riemannian geometry and geometric analysis*. Springer Verlag, 2008.

[9] J.M. Lee. *Riemannian manifolds: an introduction to curvature*, volume 176. Springer Verlag, 1997.

[10] J.M. Lee. *Introduction to smooth manifolds*, volume 218. Springer Verlag, 2003.

[11] C.B. Macdonald, J. Brandman, and S.J. Ruuth. Solving eigenvalue problems on curved surfaces using the closest point method. *Journal of Computational Physics*, 2011.

[12] C.B. Macdonald and S.J. Ruuth. Level set equations on surfaces via the closest point method. *Journal of Scientific Computing*, 35(2):219–240, 2008.

[13] C.B. Macdonald and S.J. Ruuth. The implicit closest point method for the numerical solution of partial differential equations on surfaces. *SIAM J. Sci. Comput*, 31(6):4330–4350, 2009.

[14] B. Merriman and S.J. Ruuth. Diffusion generated motion of curves on surfaces. *Journal of Computational Physics*, 225(2):2267–2282, 2007.

[15] S. Minakshisundaram. A generalization of epstein zeta functions. *Can. J. Math*, 1:320–327, 1949.

[16] S. Minakshisundaram. Eigenfunctions on riemannian manifolds. *J. Indian Math. Soc*, 17:159–165, 1953.

[17] S. Minakshisundaram and A. Pleijel. Some properties of the eigenfunctions of the laplace-operator on riemannian manifolds. *Canad. J. Math*, 1:242–256, 1949.

[18] S.J. Ruuth and B. Merriman. A simple embedding method for solving partial differential equations on surfaces. *Journal of Computational Physics*, 227(3):1943–1961, 2008.

[19] L. Tian, C.B. Macdonald, and S.J. Ruuth. Segmentation on surfaces with the closest point method. In *Image Processing (ICIP), 2009 16th IEEE International Conference on*, pages 3009–3012. IEEE, 2009.